Supplemental material to this article can be found at:
http://dmd.aspetjournals.org/content/suppl/2018/04/19/dmd.118.080408.DC2

1521-009X/46/5/719–728$35.00
DRUG METABOLISM AND DISPOSITION
https://doi.org/10.1124/dmd.118.080408
Drug Metab Dispos 46:719–728, May 2018

Special Section on Transporters in Drug Disposition and Pharmacokinetic Prediction

A Clinical Quantitative Evaluation of Hepatobiliary Transport of [^{11}C] Dehydropravastatin in Humans Using Positron Emission Tomography[S]

Ken-ichi Kaneko, Masaaki Tanaka, Akira Ishii, Yumiko Katayama, Takayoshi Nakaoka, Satsuki Irie, Hideki Kawahata, Takashi Yamanaga, Yasuhiro Wada, Takeshi Miyake, Kota Toshimoto, Kazuya Maeda, Yilong Cui, Masaru Enomoto, Etsushi Kawamura, Norifumi Kawada, Joji Kawabe, Susumu Shiomi, Hiroyuki Kusuhara, Yuichi Sugiyama, and Yasuyoshi Watanabe

RIKEN Center for Life Science Technologies (K.K., Y.K., T.N., S.I., Y.Wad., Y.C., Y.Wat.) and RIKEN Center for Molecular Imaging Sciences (Y.K., Y.Wad., Y.C., Y.Wat.), Chuo-ku, Kobe, Hyogo, Japan; Departments of Physiology, Nuclear Medicine, and Hepatology, Osaka City University Graduate School of Medicine, Abeno-ku, Osaka, Japan (M.T., A.I., H.K., T.Y., M.E., E.K., N.K., J.K., S.S.); Laboratory of Molecular Pharmacokinetics, Graduate School of Pharmaceutical Sciences, the University of Tokyo, Bunkyo-ku, Tokyo, Japan (T.M., K.M., H.K.); and Sugiyama Laboratory, RIKEN Innovation Center, RIKEN, Tsurumi-ku, Yokohama, Kanagawa, Japan (K.T., Y.S.)

Received January 7, 2018; accepted March 13, 2018

ABSTRACT

Various positron emission tomography (PET) probes have been developed to assess in vivo activities in humans of drug transporters, which aid in the prediction of pharmacokinetic properties of drugs and the impact of drug-drug interactions. We developed a new PET probe, sodium (3*R*, 5*R*)-3, 5-dihydroxy-7-((1*S*, 2*S*, 6*S*, 8*S*)-6-hydroxy-2-methyl-8- ((1-[^{11}C]-(*E*)-2-methyl-but-2-enoyl) oxy) -1, 2, 6, 7, 8, 8*a*-hexahydronaphthalen-1-yl) heptanoate ([^{11}C]DPV), and demonstrated its usefulness for the quantitative investigation of Oatps (gene symbol *SLCO*) and Mrp2 (gene symbol *ABCC2*) in rats. To further analyze the species differences and verify the pharmacokinetic parameters in humans, serial PET scanning of the abdominal region with [^{11}C]DPV was performed in six healthy volunteers with and without an OATP1Bs and MRP2 inhibitor, rifampicin (600 mg, oral), in a crossover fashion. After intravenous injection, [^{11}C]DPV rapidly distributed to the liver and kidney followed by secretion into the bile and urine. Rifampicin significantly reduced the liver distribution of [^{11}C]DPV 3-fold, resulting in a 7.5-fold reduced amount of excretion into the bile and the delayed elimination of [^{11}C]DPV from the blood circulation. The hepatic uptake clearance ($CL_{uptake,\ liver}$) and canalicular efflux clearance ($CL_{int,\ bile}$) of [^{11}C]DPV (544 ± 204 and 10.2 ± 3.5 μl/min per gram liver, respectively) in humans were lower than the previously reported corresponding parameters in rats (1800 and 298 μl/min per gram liver, respectively) (Shingaki et al., 2013). Furthermore, rifampicin treatment significantly reduced $CL_{uptake,\ liver}$ and $CL_{int,\ bile}$ by 58% and 44%, respectively. These results suggest that PET imaging with [^{11}C]DPV is an effective tool for quantitatively characterizing the OATP1Bs and MRP2 functions in the human hepatobiliary transport system.

Introduction

Multispecific transporters, such as organic anion–transporting polypeptide (OATP) 1Bs (gene symbol *SLCO*) and multidrug resistance–associated protein 2 [MRP2 (gene symbol *ABCC2*)], participate in hepatic uptake and canalicular efflux, respectively, to facilitate the excretion of a wide variety of organic anions into the bile from the blood circulation in humans (Shitara et al., 2005; Nies and Keppler, 2007; Maeda and Sugiyama, 2008; Yoshida et al., 2013). The direct measurement of drug concentrations in organs/tissue in vivo is a prerequisite for the functional characterization of drug transporters and the accurate prediction of the intrinsic clearance for overall elimination. Pharmacokinetic analyses based on plasma concentration profiles of drugs have been widely used to evaluate the overall intrinsic hepatic clearance mediated by these drug transporters. However, the elements of the overall intrinsic hepatic clearance, such as the sinusoidal uptake and the sinusoidal and canalicular efflux, are difficult to evaluate without knowing the tissue concentration time profiles of the drug in vivo. Furthermore, pharmacokinetic analyses involving the tissue concentration of a drug help to improve the quantitative investigation of drug-drug interactions (DDIs). The plasma concentrations of some drugs, the hepatic uptake of which is the rate-determining process, are not appropriate indices for assessing the changes in canalicular efflux transporters. Under such conditions, changes in the canalicular efflux transporters hardly affects the intrinsic clearance for the overall hepatic elimination, whereas liver concentrations are more profoundly altered than the plasma

This work was supported in part by a consignment expense from the Molecular Imaging Program on "Research Base for Exploring New Drugs" from the Japanese Ministry of Education, Culture, Sports, Science, and Technology (MEXT), and Japan Society for the Promotion of Science (JSPS) KAKENHI Grant-in-Aid for Scientific Research (S) [Number 24229002]. T.S. is a former employee of RIKEN Center for Life Science Technologies (CLST) and has authored several papers while at CLST.
https://doi.org/10.1124/dmd.118.080408.
[S]This article has supplemental material available at dmd.aspetjournals.org.

concentrations, depending on the changes (Watanabe et al., 2010; Maeda, 2015).

Positron emission tomography (PET) is a powerful method for quantitatively investigating the in vivo tissue distribution of drug candidates at a microdose level because of its high sensitivity and spatiotemporal resolution (Willmann et al., 2008; Kusuhara, 2013), thereby enabling the safe assessment of the pharmacokinetics of drug candidates in humans. We have established several PET probes for assessing drug transporters and demonstrated their usefulness in pharmacokinetic and DDI studies in animals (Takashima et al., 2010, 2011, 2013; Shingaki et al., 2013) and humans (Takashima et al., 2012). However, the functional characterization of multispecific drug transporters and the DDIs in vivo have not been fully analyzed to ensure the accuracy of pharmacokinetic prediction. For example, the (15*R*)-16-*m*-[^{11}C]tolyl-17, 18, 19, 20-tetranorisocarbacyclin methyl ester (15*R*-[^{11}C]TIC-Me), which was expected to be a PET probe for hepatobiliary transport, was metabolized into at least four metabolites within 20 minutes after administration (Takashima et al., 2012). Since the complicated metabolism of 15*R*-[^{11}C]TIC-Me would decrease the evaluation accuracy of drug transporter functions, nonmetabolizable PET probes are urgently required.

We recently developed a new PET probe, a pravastatin derivative, dehydropravastatin [(3*R*, 5*R*)-3, 5-dihydroxy-7-((1*S*, 2*S*, 6*S*, 8*S*)-6-hydroxy-2-methyl-8-((1-[^{11}C]-(*E*)-2-methylbut-2-enoyl) oxy)-1, 2, 6, 7, 8, 8α-hexahydronaphthalen-1-yl) heptanoate ([^{11}C]DPV)] (Fig. 1), for the quantitative characterization of the Oatps and Mrp2 functions in the hepatobiliary transport (Ijuin et al., 2012). The reliability of [^{11}C]DPV for the quantitative estimation of the Oatps and Mrp2 functions has already been demonstrated in rats using rifampicin or in Mrp2-deficient mutant rats (Shingaki et al., 2013). Rat hepatocytes produced a metabolite from [^{11}C]DPV, and human hepatocytes produced no metabolites (Shingaki et al., 2013). This finding suggests that [^{11}C]DPV is a useful PET probe for the precise evaluation of hepatobiliary transport in animals and humans.

We performed a clinical PET study with [^{11}C]DPV as a nonmetabolizable PET probe in healthy volunteers to assess the feasibility of using [^{11}C]DPV in the pharmacokinetic analysis in humans. The utility of [^{11}C]DPV PET imaging for the quantitative investigation of the drug transporters in humans was also examined using rifampicin, a well-known drug causing OATP1Bs-mediated DDIs. In addition, to confirm the membrane transport by OATP1Bs in the liver, an in vitro uptake study of DPV using OATP1B1- and OATP1B3-expressing cell lines was also conducted.

Materials and Methods

Materials. [^{11}C]DPV (Fig. 1) was synthesized at Osaka City University Hospital in accordance with the procedure reported previously (Ijuin et al., 2012). The purity and concentration of [^{11}C]DPV were assessed by high-performance liquid chromatography. The synthetic procedure for [^{11}C]DPV was validated at Osaka City University. The radiochemical purity was 100% (n = 3), and the specific radioactivity was 5.4–35.6 GBq/μmol at the time of injection. The purified fraction was evaporated and reconstituted with 5 ml of saline.

[^{3}H]Estradiol-17β-glucuronide ($E_2$17βG; 40 Ci/mmol, >97%) was purchased from PerkinElmer (Waltham, MA). Rifampicin was purchased from Sigma-Aldrich (St. Louis, MO).

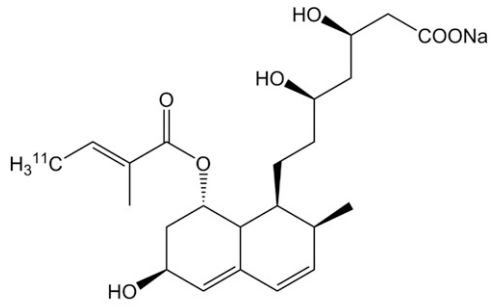

[^{11}C]DPV

Fig. 1. Chemical structure of [^{11}C]DPV.

Subjects and Study Design. The study was a single-center (Osaka City University Hospital), single-dose (microdose) clinical study. The study protocol was approved by the Ethics Committee at Osaka City University. All subjects provided their written informed consent before the study. Six healthy male Japanese subjects and a patient with Dubin-Johnson syndrome (DJS) diagnosed based on the clinical features and serum bilirubin species (Dubin and Johnson, 1954; Lee et al., 2006; van Dijk et al., 2015) were enrolled in the study. The mean ages in the healthy subjects and the DJS patient were 32 $\pm$ 9 and 67 years; the body weight and height in the healthy subjects were 65.3 $\pm$ 8.7 kg and 166.8 $\pm$ 6.1 cm, respectively, and that in the DJS patient were 59 kg and 158 cm, respectively. The subjects were allowed water but refrained from food intake for half a day before the study. Each healthy subject was enrolled for two study periods, and the DJS patient was enrolled for the first study period. In the first study period, a single intravenous bolus of [^{11}C]DPV was administered. In the second study period, a single intravenous bolus of [^{11}C]DPV was administered 1 hour after the oral administration of rifampicin (Rifadin; Daiichi-Sankyo, Tokyo, Japan) at a therapeutic dose of 600 mg (four 150-mg capsules). The dose of [^{11}C]DPV administered per body was 85.5 $\pm$ 12 MBq (chemical amount per body, 6.8 $\pm$ 4.3 nmol).

PET Scans. Dynamic scanning was performed with a PET/computed tomography Biograph Scanner (Siemens, Knoxville, TN). Before PET scanning, each subject was placed in a supine position on the scanner bed with belts attached to minimize the body movement during scanning, and then the right and left median cubital veins were cannulated for radiotracer injection and blood sampling, respectively. At the start of PET scanning, [^{11}C]DPV was intravenously administered for 30–60 seconds, and then the catheter line was flushed with 10–25 ml of saline to prevent radiotracer retention in the cannula. Serial PET scanning of the abdominal region was performed over 90 minutes in the three-dimensional dynamic mode in the following sequence: 12 $\times$ 5, 8 $\times$ 15, 4 $\times$ 30, 5 $\times$ 60, 5 $\times$ 120, 2 $\times$ 300, and 3 $\times$ 600 seconds. Blood was drawn a maximum of 13 times (at 0, 1, 2, 3, 4, 5, 6, 8, 10, 20, 30, 45, and 60 minutes after radiotracer administration). The volume of blood sampled at 0 minutes was approximately 20 ml and that at the other time points was approximately 1.5 ml. The amount of radioactivity in each sample was determined with a well-type γ-counting system (well-stand type FS-3-A; Shimadzu, Kyoto, Japan), and the data were corrected for any time decay from the point of radiotracer administration.

The Uptake of DPV by OAPT1B1- and OATP1B3-Expressing HEK293 Cells. An in vitro uptake study of DPV using empty vector–transfected and OATP1B1-expressing cells was conducted at Tsukuba Research Institute (Sekisui Medical Co. Ltd., Tokyo, Japan). The cells had been established as stably expressing OATP1B1 after lipofection of pcDNA3.1 containing an open reading frame of OATP1B1 (NM006446). An in vitro uptake study of DPV using empty vector–transfected, and OATP1B3-expressing cells was conducted as previously reported

ABBREVIATIONS: AUC, area under the concentration-time curve; $AUC_{0\text{-}t,\ blood}$, area under the concentration-time curve for blood from time 0 to time t; $AUC_{0\text{-}t}$, liver, area under the concentration-time curve for liver from time 0 to time t; [^{11}C]DPV, sodium (3*R*, 5*R*)-3, 5-dihydroxy-7-((1*S*, 2*S*, 6*S*, 8*S*)-6-hydroxy-2-methyl-8-((1-[^{11}C]-(*E*)-2-methyl-but-2-enoyl) oxy)-1, 2, 6, 7, 8, 8*a*-hexahydronaphthalen-1-yl) heptanoate; AUC_{blood}, area under the concentration-time curve for blood; $CL_{int,\ bile}$, canalicular efflux clearance; $CL_{uptake,\ kidney}$, renal uptake clearance; $CL_{uptake,\ liver}$, hepatic uptake clearance; $C_{t,\ blood}$, concentration of radioactivity as [^{11}C]DPV in the blood at time t; DDI, drug-drug interaction; DJS, Dubin-Johnson syndrome; $E_2$17βG, estradiol 17β glucuronide; K_m, Michaelis constant; MRP2/Mrp2, multidrug resistance–associated protein 2; OAT, organic anion transporter; OATP/Oatp, organic anion–transporting polypeptide; P_{dif}, clearance for passive diffusion; PET, positron emission tomography; 15*R*-[^{11}C]TIC-Me, (15*R*)-16-*m*-[^{11}C]tolyl-17, 18, 19, 20-tetranorisocarbacyclin methyl ester; TLC, thin layer chromatography; $X_{t,\ bile}$, amount of radioactivity in the sum of the amounts of radioactivity in the gallbladder and bile duct at time t; $X_{t,\ tissue}$, amount of radioactivity as [^{11}C]DPV in the liver or kidneys at time t.

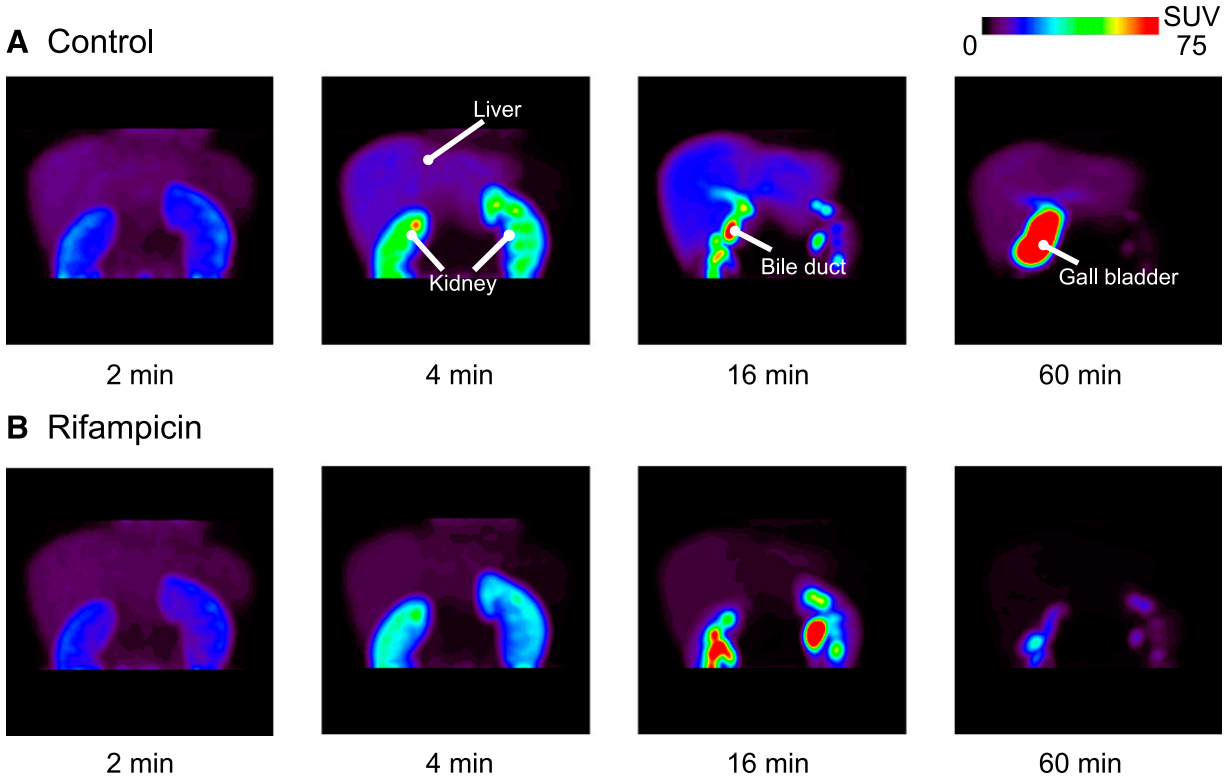

Fig. 2. Color-coded PET images of the abdominal region of healthy male subjects after the administration of [^{11}C]DPV with and without rifampicin. Coronal maximum-intensity projection PET images of the radioactivity in the abdominal region were captured at 2, 4, 10, and 60 minutes after the administration of [^{11}C]DPV (84 ± 11 MBq/body, 6.0 ± 4.0 nmol/body) in the absence (A) or presence (B) of 600 mg of rifampicin. SUV, standardized uptake value.

(Hirano et al., 2004, 2006; Matsushima et al., 2005; Kitamura et al., 2008). The amount of DPV in the uptake buffer and the cell specimens was quantified using an AB SCIEX QTRAP 5500 Mass Spectrometer (Applied Biosystems, Foster City, CA) equipped with a Prominence high-pressure liquid chromatography system (Shimadzu) operated in the negative electrospray ionization mode as previously reported (Shingaki et al., 2013). The transporter-specific uptake was determined by subtracting the uptake into vector-transfected cells from the uptake into complementary DNA-transfected cells.

Analysis of PET Imaging Data. Acquired PET image data were normalized, and all appropriate corrections were made for dead time, attenuation, and scanner calibration. The emission images were reconstructed by Fourier rebinning and two-dimensional filtered back projection with a ramp filter that had a cutoff at the Nyquist frequency (0.0 mm). Regions of interest were delineated for the liver, kidneys, bile duct, and gallbladder, which were visually identifiable, using PMOD 3.0 software (PMOD Technologies LLC, Zürich, Switzerland). For the liver and kidney images, the regions of interest were defined by calculating the radioactivity concentration and the total amount of radioactivity in the tissues. For the gallbladder and bile duct images, regions of interest that were slightly larger than the images but not overlapping the images of the other tissues, such as the liver and kidneys, were defined to calculate the total amount of radioactivity in the tissues. In this analysis, the radioactivity in the gallbladder and bile duct corresponded to that excreted into the bile. Time-radioactivity curves for each type of tissue were constructed by normalizing the decay-corrected time-radioactivity measurements to the injected dose of [^{11}C]DPV.

Radiometabolite Analyses. Radiometabolite analyses of human blood were performed using the sample obtained 2, 5, 10, 20, and 30 minutes after radiotracer administration for the PET study to confirm the production of the radiometabolites. The sample was deproteinized by precipitation with an equivalent volume of acetonitrile and centrifuged at 12,000 rpm for 2 minutes at room temperature. The supernatants of blood samples were applied to RP-8 thin layer chromatography (TLC) plates (Merck Millipore, Darmstadt, Germany). The plates were developed at room temperature with acetonitrile/water/formic acid (50:50:1) as a mobile phase. After migration, the plates were dried and exposed to BAS TR2040 imaging plates (Fujifilm Corporation, Tokyo, Japan) for 40 minutes. The distribution of radioactivity on the imaging plates was determined by digital photostimulated luminescence autoradiography using a Fuji FLA-7000 analyzer (Fujifilm Corporation) at 50-μm resolution. The data were then analyzed using MultiGauge image analysis software (Fujifilm Corporation) to calculate the proportion of parent [^{11}C]DPV.

In Vivo Kinetic Analyses to Determine Clearance on PET Imaging. The initial [^{11}C]DPV uptake clearance was calculated for the human liver or kidneys by the integration plot method (Kim et al., 1988), using the portion of time-radioactivity curves encompassing the linear range of the plot after [^{11}C]DPV administration, during which the effects of the metabolism and excretion from the tissue were negligible. The uptake clearance of [^{11}C]DPV was determined using eq. 1:

$$\frac{X_{t,\ tissue}}{C_{t,\ blood}} = CL_{uptake,\ tissue} \times \frac{AUC_{0\text{-}t,\ blood}}{C_{t,\ blood}} + V_{E,\ tissue} \bullet\bullet\bullet \quad (1)$$

where $X_{t,\ tissue}$ is the amount of radioactivity as [^{11}C]DPV in the liver or kidneys at time t, as determined by PET imaging, and $C_{t,\ blood}$ is the concentration of radioactivity as [^{11}C]DPV in the blood at time t, as determined by γ-counter measurement of the radioactivity in the blood taken from the femoral artery. The tissue uptake clearance [hepatic uptake clearance ($CL_{uptake,\ liver}$) and renal uptake clearance ($CL_{uptake,\ kidney}$)] was obtained from the initial slope of the plot of $X_{t,\ tissue}/C_{t,\ blood}$ versus the $AUC_{0\text{-}t,\ blood}/C_{t,\ blood}$, where $AUC_{0\text{-}t,\ blood}$ is the area under the concentration-time curve (AUC) for blood (AUC_{blood}) from time 0 to time t. $V_{E,\ tissue}$ represents the initial distribution volume in the liver or kidneys at time 0, calculated from the y-intercept of the plot.

The canalicular efflux clearance with regard to the liver radioactivity ($CL_{int,\ bile}$) was estimated using the following equation by noninvasive measurements of the radioactivity in the gallbladder and bile duct (the radioactivity excreted into the bile):

$$X_{t,\ bile} = CL_{int,\ bile} \times AUC_{0\text{-}t,\ liver} + V_E \bullet\bullet\bullet \quad (2)$$

where $X_{t,\ bile}$ is the amount of radioactivity in the sum of the amounts of radioactivity in the gallbladder and bile duct at time t, as determined by PET imaging. In the control phase, significant radioactivity was also detected in the small intestines of volunteers 1 and 3, who did not show any radioactivity in the small intestine in the rifampicin-treated phase. We speculated that the radioactivity (1% and 18% of $X_{t,\ bile}$, respectively) originated from the bile and, thus, was added to $X_{t,\ bile}$ values in the analysis. $AUC_{0\text{-}t,\ liver}$ is the AUC for liver from time

0 to time t. The $CL_{int,\ bile}$ value can be obtained from the slope of the plot of $X_{t,\ bile}$ versus $AUC_{0\text{-}t,\ liver}$. V_E was calculated as the *y*-intercept of the integration plot.

Calculations for the In Vitro Kinetic Parameters in the Uptake Study Using Transporter-Expressing Cells. The concentration dependence on the uptake velocity of DPV by OATP1B1 and OATP1B3 was fitted to the Michaelis-Menten equation, as follows:

$$\nu = \frac{V_{max} \cdot S}{K_m + S} + P_{dif} \cdot S \quad \bullet\bullet\bullet \tag{3}$$

where ν is the uptake rate of the substrate (pmol/min per milligram of protein), S is the substrate concentration in the medium (μM), K_m is the Michaelis constant (μM), V_{max} is the maximum uptake rate (pmol/min per milligram protein), and P_{dif} is the clearance for nonsaturable component (ml/min per milligram protein). For OATP1B1, S was not included in the parameter estimation. In the parameter estimation of K_m and V_{max} values for OATP1B3, P_{dif} was fixed as the uptake clearance at the highest concentration, 0.433 μl/min per milligram of protein. This uptake value was identical to the uptake clearance of DPV in the empty vector–transfected cells.

Statistical Analyses. Data were calculated as the mean ± S.D. for six determinations. Student's two-tailed paired *t* test was used to identify significant differences between the control group and the rifampicin-treated group. A two-way analysis of variance with the Bonferroni multiple comparisons test was used to assess the effect of rifampicin on the time profiles of tissue radioactivity. Statistical significance was set at $P < 0.05$.

Results

Biodistribution of Radioactivity in the Human Abdominal Region and Blood After the Intravenous Administration of [^{11}C]DPV. Representative PET images of [^{11}C]DPV in abdominal tissues with and without rifampicin treatment in the healthy subjects are shown in Fig. 2. Representative PET images of [^{11}C]DPV in abdominal tissues without rifampicin treatment in the healthy subjects and the DJS patient are shown in Fig. 7. The distribution of [^{11}C]DPV was observed in the liver and kidney and was negligible in the other tissues (Supplemental Fig. 1).

The time profiles of the mean total tissue and blood radioactivity and AUC_{blood} are shown in Fig. 3 and Table 1. Radioactivity peaked at 0.0237% ± 0.003% of the dose in the livers of control subjects at 13 minutes after administration and 0.0080% ± 0.0013% of the dose in the liver of rifampicin-treated subjects at 1.9 minutes after administration. Rifampicin treatment significantly reduced the amount of radioactivity excreted into the bile (1.5% ± 1.0% of the dose in rifampicin-treated subjects versus 11.2% ± 2.7% of the dose in control subjects), and delayed the elimination of radioactivity from the systemic circulation (Fig. 3). Consequently, the AUC_{blood} values in rifampicin-treated subjects were 1.7-fold higher than those in control subjects (0.180% ± 0.061% versus 0.103% ± 0.020% of the dose·minutes per milliliter) (Table 1). In contrast, rifampicin treatment slightly delayed the elimination of radioactivity from the kidney, resulting in an increase in the AUC for the kidney (Table 1).

The time profiles of the mean total tissue and blood radioactivity in the healthy subjects and the DJS patient are shown in Figs. 3 and 8. Radioactivity peaked at 0.0237% ± 0.003% of the dose in the livers of healthy subjects at 13 minutes after administration, and at 0.0164% of the dose in the liver of DJS patient at 17 minutes after administration. The amount of radioactivity in the DJS patient excreted into the bile was less than that in healthy subjects (3.88% of the dose in the DJS patient versus 11.2% ± 2.7% of the dose in healthy subjects) (Fig. 8). The AUC_{blood} values in the DJS patient were slightly higher than those in healthy subjects (0.137% versus 0.103% ± 0.020% of the dose·minutes per milliliter).

Radiometabolite Analyses of [^{11}C]DPV in the Blood by TLC Autoradiography. Figure 4 shows representative TLC autoradiograms of extracts from the blood by 30 minutes after the administration of [^{11}C]DPV to the control and rifampicin-treated subjects. A TLC analysis revealed one identifiable metabolite (M1) with [^{11}C]DPV in the blood in all groups.

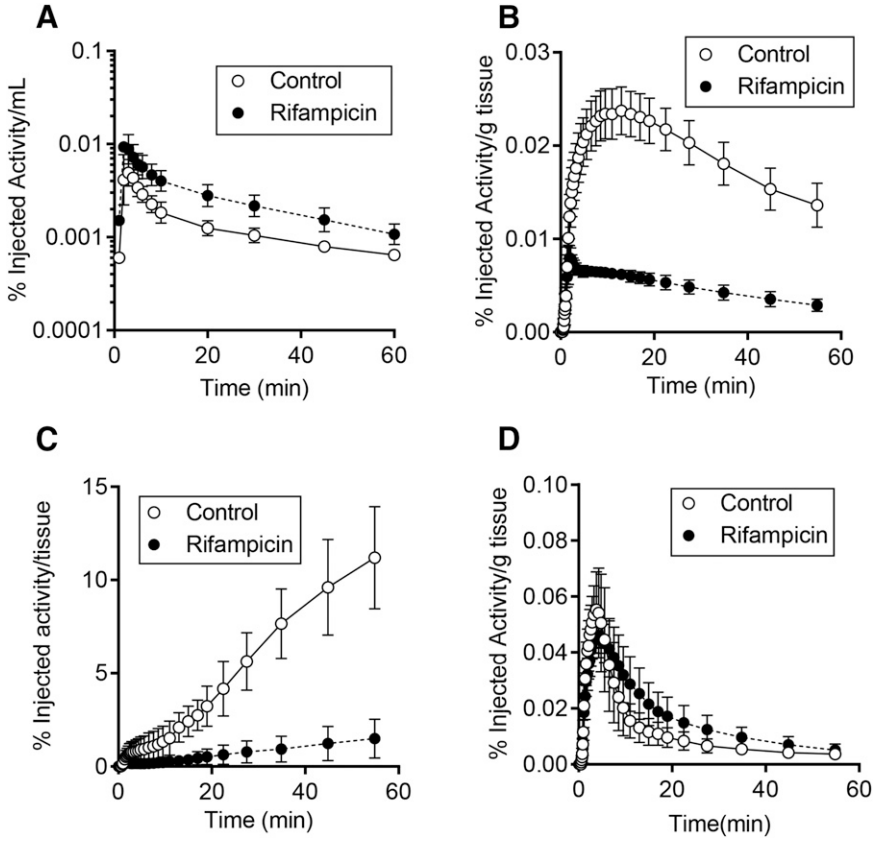

Fig. 3. Radioactivity-time profiles in the blood, liver, and kidneys of healthy male subjects after the intravenous administration of [^{11}C]DPV. Time profiles of the mean ± S.D. (n = 6) radioactivity in the blood (A), liver (B), gallbladder and bile duct (C), and kidney (D) were determined. PET imaging of the abdominal region and blood sampling were performed over 60 minutes after the administration of [^{11}C]DPV to subjects who received (closed circles) or did not receive (open circles) rifampicin pretreatment.

TABLE 1

Pharmacokinetic parameters of [^{11}C]DPV after intravenous administration in control and rifampicin subjects

$CL_{uptake,\ liver}$, $CL_{uptake,\ kidneys}$, $V_{E,\ liver}$, and $V_{E,\ kidneys}$ were calculated from eq. 1, and $CL_{int,\ bile}$ was obtained from eq. 2. Values are the mean ± S.D. (n = 6), unless otherwise indicated. The unit of clearance determined by the integration plot analysis was converted using the body weight, liver weight, and kidney weight in Supplemental Table 1.

	Control	Rifampicin Treated	Rifampicin Treated/Control (%)
$AUC_{0-60\ min,\ blood}$ (%dose·min per milliliter)	0.103 ± 0.020	0.180 ± 0.061**	174.8
$AUC_{0-60\ min,\ liver}$ (%dose·min per gram of tissue)	1.02 ± 0.11	0.263 ± 0.034***	25.8
$AUC_{0-60\ min,\ kidney}$ (%dose·min per gram of tissue)	0.656 ± 0.197	0.906 ± 0.259	138.1
$CL_{uptake,\ liver}$ (ml/min per kilogram)	11.4 ± 4.0	5.18 ± 3.81**	45.4
$V_{E,\ liver}$ (ml/kg)	4.45 ± 0.63	4.07 ± 0.84	91.5
$CL_{uptake,\ kidney}$ (ml/min per kilogram)	7.83 ± 3.26	5.72 ± 3.80	73.1
$V_{E,\ kidneys}$ (ml/kg)	5.49 ± 0.67	5.44 ± 0.47	99.1
$CL_{int,\ bile}$ (ml/min per kilogram)	0.221 ± 0.083	0.129 ± 0.091*	58.4

$AUC_{0-60\ min,\ blood}$, AUC for blood from 0 to 60 min; $AUC_{0-60\ min,\ kidney}$, AUC for kidney from 0 to 60 min; $AUC_{0-60\ min,\ liver}$ before AUC for liver from 0 to 60 min; $V_{E,\ kidneys}$, V_E in the kidneys; $V_{E,\ liver}$, V_E in the liver.

*$P < 0.05$; **$P < 0.01$; ***$P < 0.0001$, statistical significance was tested by Student's two-tailed paired t test.

The abundance of parent [^{11}C]DPV in the blood (percentage of the total activity applied) in the control subjects ($n = 6$) was 100% at 2 and 5 minutes, and decreased with time, as follows: 87% ± 17% at 10 minutes, 70% ± 13% at 20 minutes, and 63% ± 16% at 30 minutes. The abundance of parent [^{11}C]DPV in the blood of rifampicin-treated subjects ($n = 6$) showed profiles similar to those of the control subjects, as follows: 100% at 2 minutes, 98% ± 4% at 5 minutes, 97% ± 4% at 10 minutes, 85% ± 14% at 20 minutes, and 86% ± 14% at 30 minutes, respectively. Overall, the TLC assay with blood samples suggests that similar parent [^{11}C]DPV profiles in the blood were exhibited by all groups and that the treatment by rifampicin was likely to have negligible effects on the metabolism of [^{11}C]DPV.

The Liver Uptake and Canalicular Efflux Clearance of [^{11}C] DPV. Integration plots were drawn to calculate the tissue uptake clearance of radioactivity (Figs. 5 and 8). The slopes of the plots were determined across the linear range. $CL_{uptake,\ liver}$ values in the control subjects ranged from 32% to 76% of the hepatic blood flow rate (21 ml/min per kilogram) (Davies and Morris, 1993). Rifampicin treatment significantly decreased the $CL_{uptake,\ liver}$ value (by 58% ± 19%; $P < 0.01$) compared with that in control subjects, but had no effect on $CL_{uptake,\ kidney}$, which was 7.83 ± 3.26 and 5.72 ± 3.80 ml/min per kilogram, respectively, in control and rifampicin-treated subjects.

Integration plots were also performed to determine the $CL_{int,\ bile}$ values of radioactivity across the linear range. Rifampicin treatment resulted in significant 40% lower $CL_{int,\ bile}$ values (0.129 ± 0.091 versus 0.221 ± 0.083 ml/min per kilogram, respectively) in rifampicin-treated subjects than in control subjects (Table 1), although its inhibitory effect varied from 8.6% to 87% depending on the volunteers. More than 30% reduction was observed in four of six subjects. Further, the $CL_{int,\ bile}$ values in the DJS patient was lower than that in the healthy subjects (0.102 versus 0.221 ± 0.083 ml/min per kilogram, respectively).

The Uptake of DPV by OATP1B1- and OATP1B3-Expressing HEK293 Cells. The activities of OATP1B1 and OATP1B3 in HEK293 cells were confirmed by examining the uptake of [^{3}H]$E_2$17βG, a prototypical substrate of OATPs, in the presence and absence of rifampicin (100 μM). The uptake of [^{3}H]$E_2$17βG in the OATP1B1- and OATP1B3-expressing cells was significantly decreased in the presence of rifampicin (Supplemental Fig. 2). DPV (1 and 3 μM, respectively, for OATP1B1 and OATP1B3 tests) was significantly accumulated in both OATP1B1- and OATP1B3-expressing cells but was diminished in the presence of rifampicin (10 μM) (Fig. 6). The uptake rate of DPV in OATP1B1- and OATP1B3-expressing cells was determined at various substrate concentrations (3–300 μM) (Fig. 6). The uptake velocity of DPV by OATP1B1 and OATP1B3 follows the Michaelis-Menten equation. The K_m (micromolar) and V_{max} values of DPV were 6.52 ± 2.16 and 42.1 ± 3.2 pmol/min per milligram of protein for OATP1B1, and 17.1 ± 8.3 and 39.6 ± 12.1 pmol/min per milligram of protein for OATP1B3, respectively.

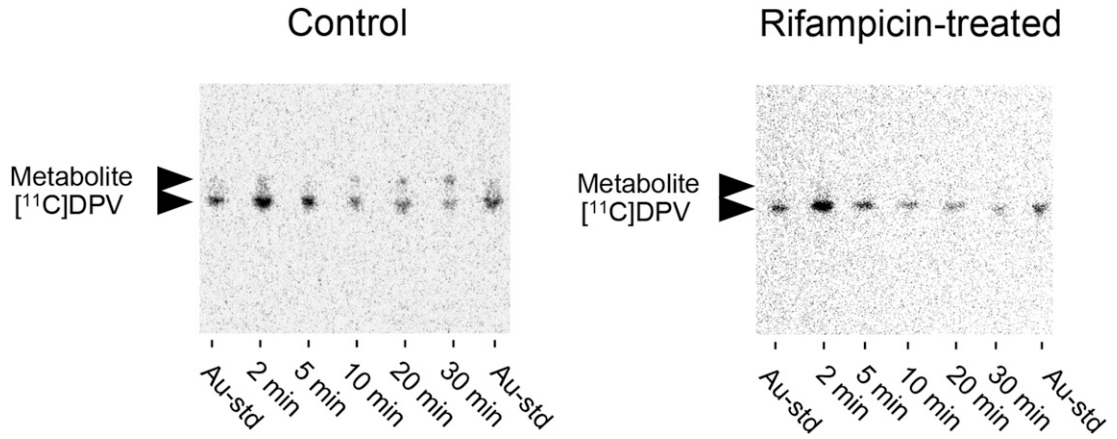

Fig. 4. Representative radiochromatograms of [^{11}C]DPV and its metabolites in blood. Blood specimens collected from control and rifampicin-treated subjects at 2, 5, 10, 20, and 30 minutes were subjected to TLC and then analyzed by autoradiography. Au-std, [^{11}C]DPV as an authentic standard.

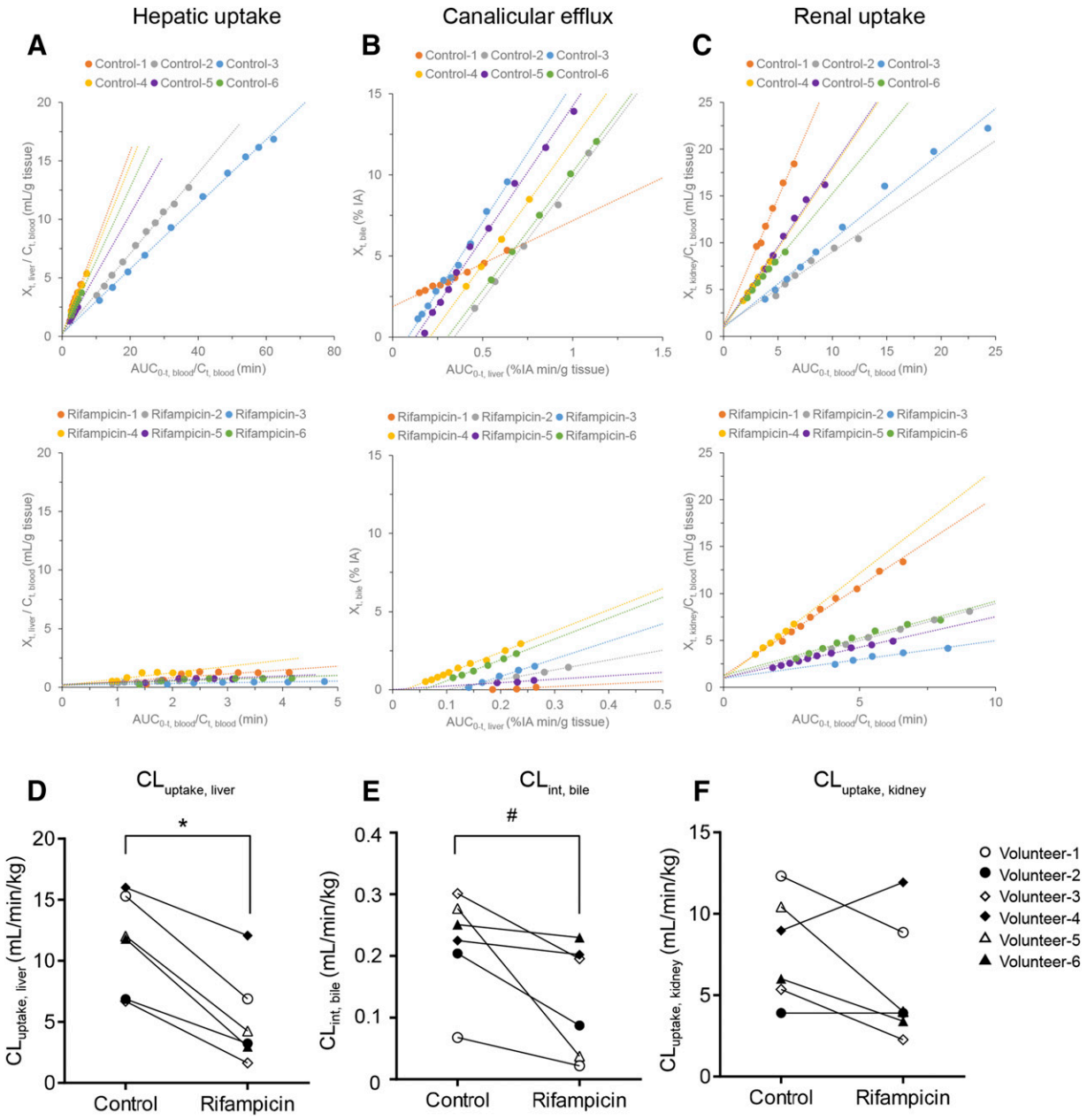

Fig. 5. An integration plot analysis after the intravenous administration of [^{11}C]DPV. Integration plots were determined for the hepatic uptake (A), canalicular efflux (B), and renal uptake (C) clearance of [^{11}C]DPV in the control and rifampicin-treated (600 mg/body) subjects. The hepatic uptake (D), canalicular efflux (E), and renal uptake (F) clearance were compared between the control and rifampicin-treated groups. The statistical significance was tested by Student's two-tailed paired *t* test (#$P < 0.05$; *$P < 0.01$).

Discussion

We demonstrated that [^{11}C]DPV, a newly developed PET probe, was a useful novel noninvasive method of assessing the activity of in vivo drug transporters in humans. We showed that PET imaging with [^{11}C]DPV enabled the quantitative evaluation of the function of OATP1Bs in hepatic uptake, and of MRP2 in canalicular efflux. This helped to clarify the drug transporter–mediated DDIs.

Hepatic and/or renal elimination is the major pathway of most drugs in a living body. Since multispecific drug transporters, such as OATP1Bs and organic anion transporters (OATs), are indispensable in the hepatic and renal uptake of various drugs, especially those with anionic properties, the accurate functional characterization of these transporters is essential to drug development. Noninvasive PET imaging methods potentially offer new approaches to the direct estimation of the functional activity of transporters that contribute to drug disposition, even in humans. Indeed, through their PET imaging–based pharmacokinetic analysis, Takashima et al. (2010, 2012) demonstrated that 15*R*-[^{11}C]TIC was an OATP1Bs transporter substrate in rat and human livers and directly estimated the pharmacokinetic parameters of $CL_{uptake,\ liver}$. The $CL_{uptake,\ liver}$ in humans was one-third of that in rats. The magnitude of the relationship between $CL_{uptake,\ liver}$ and the hepatic blood flow rate showed a clear species difference; the $CL_{uptake,\ liver}$ in rats was comparable to the hepatic blood flow rate (55 ml/min per kilogram), whereas that in humans was below the hepatic blood flow rate (Takashima et al., 2012). A large amount of the multiple metabolites

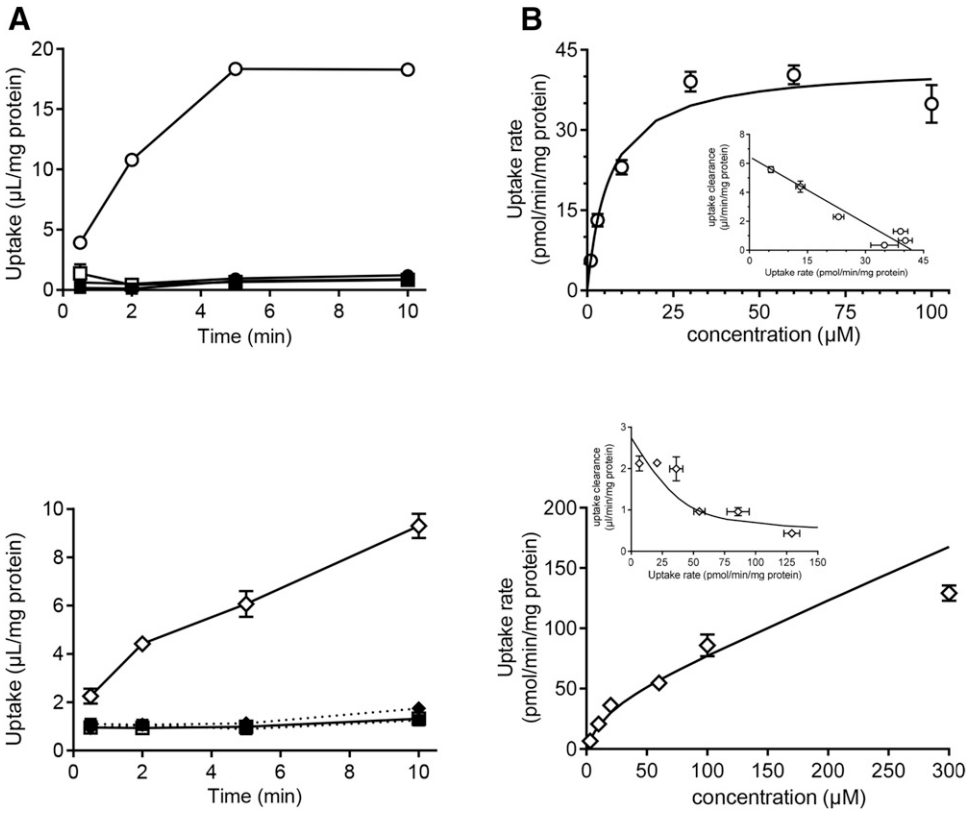

Fig. 6. The uptake of DPV by OATP1B1- and OATP1B3-expressing HEK293 cells. (A) The uptake of DPV (1 and 3 μM, respectively, for OATP1B1 and OATP1B3 tests) by empty vector–transfected cells (square symbol), OATP1B1-expressing cells (circle symbol), and OATP1B3-expressing cells (diamond symbol) in the absence (open symbol) and presence (closed symbol) of rifampicin (10 μM) was determined at 37°C at the designated time points. (B) The concentration dependence of the uptake is shown as a Michaelis-Menten plot and Eadie-Hofstee plot (inset). The uptake of DPV for 2 minutes was determined at various substrate concentrations (1–100 μM for OATP1B1, and 3–300 μM for OATP1B3). Solid lines represent the fitted lines. Details of the fitting are described in *Materials and Methods*. Each point represents the mean ± S.E. (n = 4 for OATP1B1; n = 3 for OATP1B3).

(rats, three metabolites; humans, four metabolites) of 15*R*-[^{11}C]TIC-Me in liver might have hampered the precise evaluation of the hepatobiliary clearance in vivo (Takashima et al., 2010, 2012).

We found that the distribution of the pravastatin analog [^{11}C]DPV is limited to the liver and kidney in humans, as previously reported in rats (Shingaki et al., 2013). Rifampicin treatment markedly decreased the

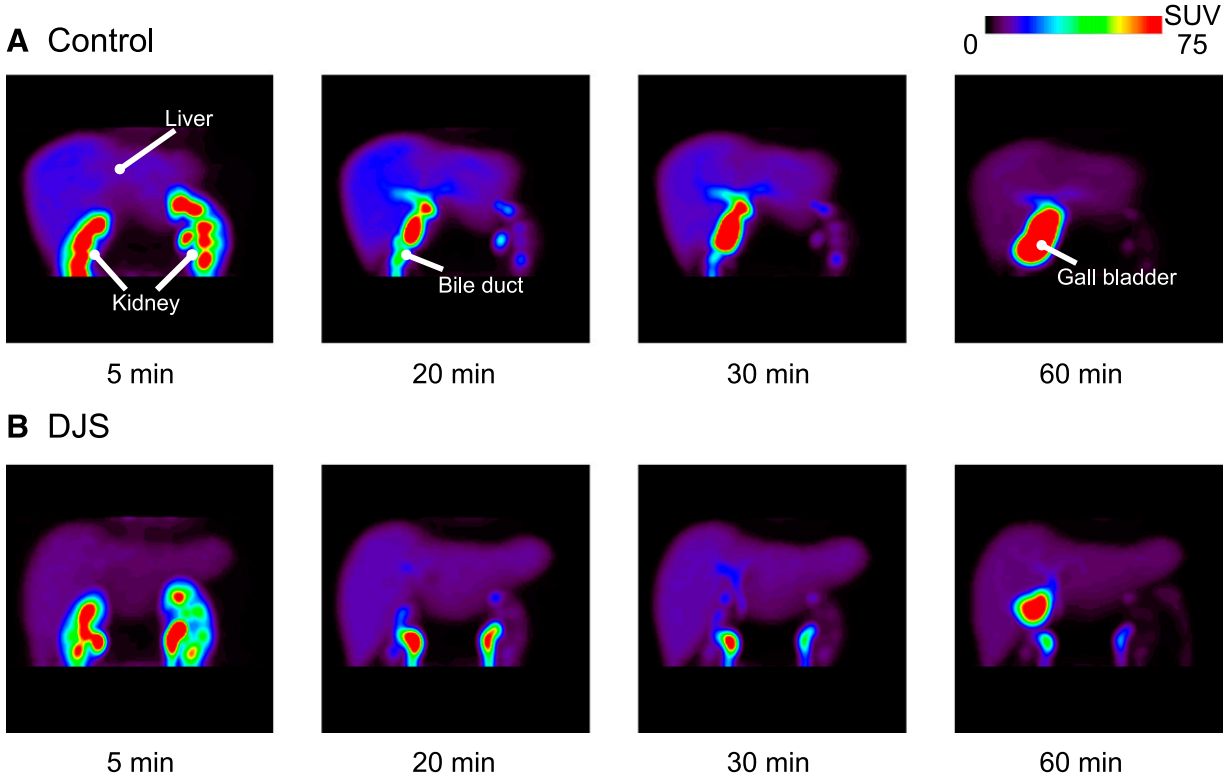

Fig. 7. Color-coded PET images of the abdominal region of healthy male subjects (A) and a DJS patient (B) after the administration of [^{11}C]DPV. Coronal maximum-intensity projection PET images of the radioactivity in the abdominal region were captured at 5, 20, 30, and 60 minutes after the administration of [^{11}C]DPV (82 ± 12 MBq/body, 8.7 ± 5.0 nmol/body). SUV, standardized uptake value.

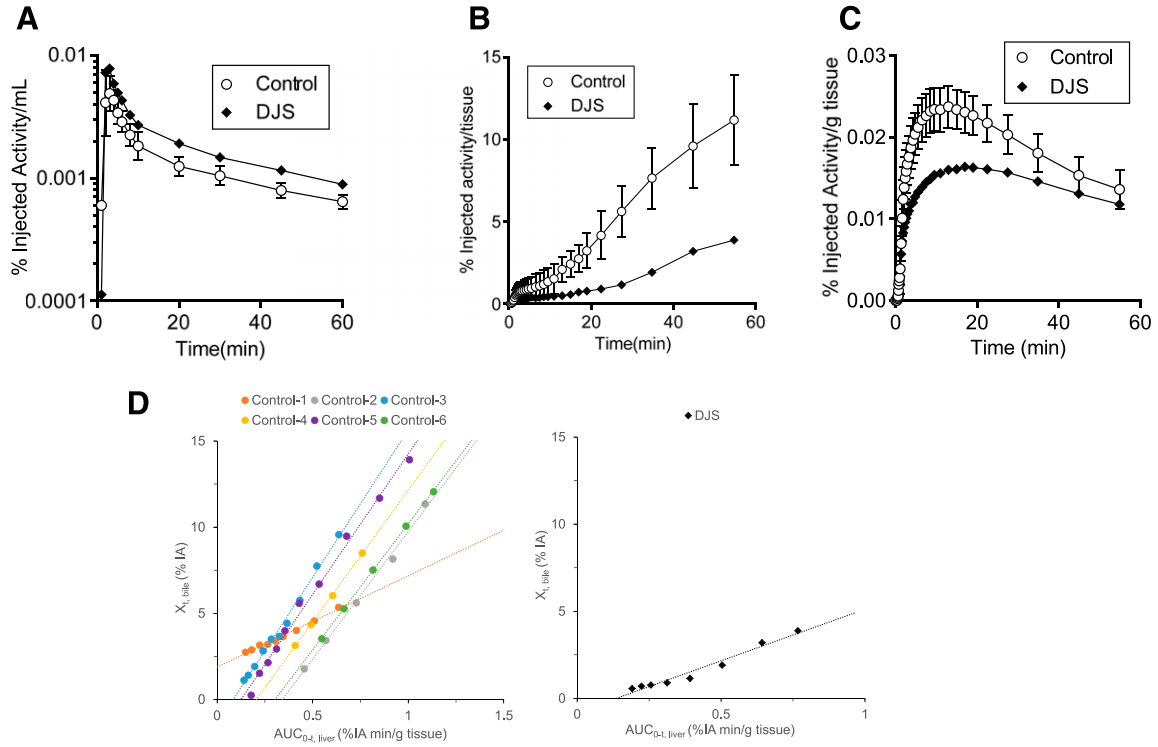

Fig. 8. Radioactivity-time profiles of the blood, liver, and gallbladder and bile duct, and integration plot analysis of the gallbladders and bile ducts of healthy male subjects and a DJS patient after the intravenous administration of [^{11}C]DPV. The time profile of the mean ± S.D. radioactivity in the blood (A), liver (B), and gallbladder and bile duct (C) of control subjects (n = 6) was determined. The time profile of the DJS patient was the data from a single patient. PET imaging of the abdominal region and blood sampling were performed over 60 minutes after the administration of [^{11}C]DPV to the control subjects (open circles) or the DJS patient (closed diamonds). (D) Integration plots were determined for the canalicular efflux clearance of [^{11}C]DPV in the control subjects and the DJS patient. Closed circles represent the control subjects. Closed diamonds represent the DJS patient.

liver radioactivity, and its AUC, and reduced the cumulative radioactivity of [^{11}C]DPV associated with the gallbladder and bile duct (Fig. 3; Table 1). Consequently, rifampicin significantly delayed the elimination of radioactivity from the blood (Fig. 3; Table 1). Although rifampicin treatment did not affect the maximum radioactivity in the kidney, a slight delay caused by prolonged systemic exposure was observed. These changes were in good agreement with the clinical studies of 15*R*-[^{11}C]TIC (Takashima et al., 2012), suggesting that hepatic elimination accounts for a significant fraction of the total elimination pathway of [^{11}C]DPV from the blood circulation.

The tissue uptake clearances ($CL_{uptake,\ liver}$ and $CL_{uptake,\ kidney}$), regarding the blood concentrations, and intrinsic canalicular efflux ($CL_{int,\ bile}$), regarding the liver concentrations, were determined by an integration plot analysis. Rats exhibited a blood flow–limited liver uptake of [^{11}C]DPV (Shingaki et al., 2013). Meanwhile, the $CL_{uptake,\ liver}$ was half of the human hepatic blood flow rate (20.7 ml/min per kilogram) (Table 1). $CL_{uptake,\ liver}$ values in humans (544 ± 204 μl/min per gram of liver) were 3-fold lower than the previously reported corresponding parameters in rats (1800 μl/min per gram of liver). Considering the blood flow–limited liver uptake in rats, the species difference in the intrinsic tissue uptake clearances will be more remarkable. The $CL_{uptake,\ liver}$ value of [^{11}C]DPV was almost equivalent to the nonrenal clearance (7.2 ml/min per kilogram) of pravastatin in humans (Singhvi et al., 1990). This is consistent with in vitro data, where the transport activities of DPV and pravastatin by OATP1B1 and OATP1B3 were similar (Supplemental Fig. 3). Further, the K_m value for OATP1B1 was almost the same as that of pravastatin, as reported previously (27, 29, and 35 μM, respectively) (Hsiang et al., 1999; Sharma et al., 2012; Izumi et al., 2015). More importantly, significant reduction in the $CL_{uptake,\ liver}$ of [^{11}C]DPV by rifampicin administration supports (Fig. 5) that this PET tracer is applicable for the quantitative evaluation of the human hepatic uptake mediated by OATP1B1 and OATP1B3. Meanwhile, the modest effect of rifampicin (Table 1) suggests that it is necessary to validate the dynamic range for the analysis.

Although a PET imaging–based pharmacokinetic analysis allows for the quantitative evaluation of $CL_{int,\ bile}$, it is limited by its inability to distinguish between the radioactivity of the parent drug and its metabolites in the targeted tissue. [^{11}C]DPV is hardly metabolized in in vitro human hepatocytes (Shingaki et al., 2013), whereas our radiometabolite analysis in humans confirmed the presence of a metabolite (M1) with radioactivity in the blood. The abundance of the M1 in the control subjects (n = 6) increased with time and accounted for approximately 40% of the total activity at 30 minutes after administration. Since one metabolite predominated in the blood 20 minutes after the injection of 15*R*-[^{11}C]TIC-Me (Takashima et al., 2012), [^{11}C]DPV is a more metabolically stable PET probe than 15*R*-[^{11}C]TIC-Me. However, the impact of metabolite formation on the evaluation of $CL_{int,\ bile}$ values of [^{11}C]DPV remains unknown. Further studies are necessary to identify M1, and to clarify the MRP2 activities of the M1 in comparison with DPV to increase the certainty of $CL_{int,\ bile}$ measurement. Concurrently, we continue our efforts to develop a nonmetabolizable PET probe for OATP1Bs and MRP2.

The functional activity of Mrp2 in rats was evaluated based on a [^{11}C]DPV PET imaging analysis. Rifampicin-treated and Mrp2-defective rats showed decreased $CL_{int,\ bile}$ (Shingaki et al., 2013). Large differences are seen in the liver MRP2 activity of rats and other species, including humans (Ishizuka et al., 1999; Niinuma et al., 1999).

The ATP-dependent uptake of pravastatin by the canalicular membrane vesicles in humans was six times lower than that in rats (Niinuma et al., 1999). Consistently, the $CL_{int, bile}$ of [^{11}C]DPV (10.2 μl/min per gram of liver) in control subjects was 30 times lower than those in rats (298 μl/min per gram of liver) (Shingaki et al., 2013). The effect of rifampicin on the $CL_{int, bile}$ was statistically significant, but varied; the value decreased by >30% in four of six subjects, whereas the others showed a reduction of ≤10%. To strengthen the application of [^{11}C]DPV as a PET probe for MRP2, an additional clinical study was conducted in a patient with DJS caused by hereditary MRP2 deficiency. The $CL_{int, bile}$ in the DJS patient (0.102 ml/min per kilogram) was smaller than that in control subjects (0.221 ml/min per kilogram) (Figs. 7 and 8), supporting the importance of MRP2 in the transport process. The impact of genetic polymorphisms of OATP1Bs and MRP2 on the pharmacokinetic parameters remains to be clarified by [^{11}C]DPV PET imaging, because the pharmacokinetics of pravastatin showed large interindividual variation due to genetic polymorphisms of not only OATP1Bs but also MRP2 (Ieiri et al., 2009).

Since DPV is efficiently transported by OAT3, but not by OAT1 (Supplemental Fig. 4), this transporter will mediate the basolateral uptake in the kidney, as suggested for pravastatin (Watanabe et al., 2011). $CL_{uptake, kidney}$ was decreased in four of six subjects by rifampicin treatment (Fig. 5). The factor accounting for the interindividual variability in the effect of rifampicin remains unknown. Such interindividual variability was also observed to a lesser extent in the renal clearance of pravastatin, which was decreased in 3 of 10 subjects (Kyrklund et al., 2004). Provided that rifampicin is a weak inhibitor of OAT3 (Kusuhara et al., 2013), the inhibition of OAT3-mediated uptake is an unlikely mechanism.

This study highlighted the usefulness of PET imaging in investigating pharmacokinetics and DDIs, particularly in the tissue concentrations caused by the inhibition of the transporter function. The tissue concentration of drugs is associated with the drug response when an intracellular protein is the target. However, when the uptake involves transporters, the prediction of the tissue concentration under both control and DDI conditions must be further clarified. A clinical PET study could determine the tissue concentration when the drug is labeled by a positron-emitted isotope. Furthermore, pharmacokinetic analyses of the PET data will help to clarify the DDI mechanisms, including some that may have been overlooked. Indeed, the present study suggests that the DDI mechanisms of rifampicin involve the inhibition of the canalicular efflux in some patients, as well as the sinusoidal uptake by OATP1B1/OATP1B3. There are two factors accounting for interindividual variability in $CL_{int, bile}$ to be investigated: the interindividual difference in MRP2 sensitivity to rifampicin caused by its genetic polymorphisms; and that in the unbound liver concentration of rifampicin caused by interindividual difference in the membrane transport and metabolism. Moreover, the accumulation of data on the in vivo intrinsic parameters of the elements across the drugs will provide correlations to in vitro parameters and help identify the empirical scaling factors that may improve the precision of the in vitro-in vivo extrapolation to new chemical entities. Molecular imaging probes for the quantitative functional characterization of drug transporters are still being developed by our group and others [[^{11}C]rosuvastatin, Oatps, Bcrp (breast cancer resistance protein), and Mrp2 in rats] (He et al., 2014), but the characterization of drug transporters and DDIs in humans has not yet been fully achieved. Further enrichment of these probes is necessary to increase the predictability of these transporters.

In conclusion, our findings demonstrated that noninvasive PET imaging with [^{11}C]DPV as a PET probe with fewer metabolites than 15*R*-[^{11}C]TIC-Me can assess the hepatobiliary transport by OATP1Bs and MRP2. Therefore, [^{11}C]DPV is a useful probe for the kinetic analysis of hepatobiliary transport in humans.

Acknowledgments

The authors thank the investigators and subjects who participated in this study for valuable help and cooperation; as well as Tomotaka Shingaki, formerly of CLST, for clinical support. We also thank Masashi Okamoto and Hisako Kobata (Osaka City University Hospital) for expert technical assistance and supervision of this study, and Ryo Fujino and Shunske Aoyama (ADME & Toxicology Research Institute, Sekisui Medical Co., Ltd., Ibaraki, Japan) for contributing to in vitro experiments using HEK293 cells expressing OATP1B1.

Authorship Contributions

Participated in research design: Kaneko, Maeda, Enomoto, Kawamura, Kawada, Kusuhara, Sugiyama, Watanabe.

Conducted experiments: Tanaka, Ishii, Katayama, Kawahata, Yamanaga, Wada, Miyake.

Contributed new reagents or analytic tools: Tanaka, Katayama, Kawahata, Yamanaga, Wada, Kawabe, Shiomi.

Performed the data analysis: Kaneko, Katayama, Nakaoka, Irie, Miyake, Toshimoto.

Wrote or contributed to the writing of the manuscript: Kaneko, Maeda, Cui, Kusuhara, Sugiyama, Watanabe.

References

Davies B and Morris T (1993) Physiological parameters in laboratory animals and humans. *Pharm Res* **10**:1093–1095.

Dubin IN and Johnson FB (1954) Chronic idiopathic jaundice with unidentified pigment in liver cells; a new clinicopathologic entity with a report of 12 cases. *Medicine (Baltimore)* **33**:155–197.

He J, Yu Y, Prasad B, Link J, Miyaoka RS, Chen X, and Unadkat JD (2014) PET imaging of Oatp-mediated hepatobiliary transport of [(^{11})C] rosuvastatin in the rat. *Mol Pharm* **11**:2745–2754.

Hirano M, Maeda K, Shitara Y, and Sugiyama Y (2004) Contribution of OATP2 (OATP1B1) and OATP8 (OATP1B3) to the hepatic uptake of pitavastatin in humans. *J Pharmacol Exp Ther* **311**:139–146.

Hirano M, Maeda K, Shitara Y, and Sugiyama Y (2006) Drug-drug interaction between pitavastatin and various drugs via OATP1B1. *Drug Metab Dispos* **34**:1229–1236.

Hsiang B, Zhu Y, Wang Z, Wu Y, Sasseville V, Yang WP, and Kirchgessner TG (1999) A novel human hepatic organic anion transporting polypeptide (OATP2). Identification of a liver-specific human organic anion transporting polypeptide and identification of rat and human hydroxymethylglutaryl-CoA reductase inhibitor transporters. *J Biol Chem* **274**:37161–37168.

Ieiri I, Higuchi S, and Sugiyama Y (2009) Genetic polymorphisms of uptake (OATP1B1, 1B3) and efflux (MRP2, BCRP) transporters: implications for inter-individual differences in the pharmacokinetics and pharmacodynamics of statins and other clinically relevant drugs. *Expert Opin Drug Metab Toxicol* **5**:703–729.

Ijuin R, Takashima T, Watanabe Y, Sugiyama Y, and Suzuki M (2012) Synthesis of [(^{11})C]-dehydropravastatin, a PET probe potentially useful for studying OATP1B1 and MRP2 transporters in the liver. *Bioorg Med Chem* **20**:3703–3709.

Ishizuka H, Konno K, Shiina T, Naganuma H, Nishimura K, Ito K, Suzuki H, and Sugiyama Y (1999) Species differences in the transport activity for organic anions across the bile canalicular membrane. *J Pharmacol Exp Ther* **290**:1324–1330.

Izumi S, Nozaki Y, Maeda K, Komori T, Takenaka O, Kusuhara H, and Sugiyama Y (2015) Investigation of the impact of substrate selection on *in vitro* organic anion transporting polypeptide 1B1 inhibition profiles for the prediction of drug-drug interactions. *Drug Metab Dispos* **43**:235–247.

Kim DC, Sugiyama Y, Satoh H, Fuwa T, Iga T, and Hanano M (1988) Kinetic analysis of *in vivo* receptor-dependent binding of human epidermal growth factor by rat tissues. *J Pharm Sci* **77**:200–207.

Kitamura S, Maeda K, Wang Y, and Sugiyama Y (2008) Involvement of multiple transporters in the hepatobiliary transport of rosuvastatin. *Drug Metab Dispos* **36**:2014–2023.

Kusuhara H (2013) Imaging in the study of membrane transporters. *Clin Pharmacol Ther* **94**:33–36.

Kusuhara H, Miura M, Yasui-Furukori N, Yoshida K, Akamine Y, Yokochi M, Fukizawa S, Ikejiri K, Kanamitsu K, Uno T, et al. (2013) Effect of coadministration of single and multiple doses of rifampicin on the pharmacokinetics of fexofenadine enantiomers in healthy subjects. *Drug Metab Dispos* **41**:206–213.

Kyrklund C, Backman JT, Neuvonen M, and Neuvonen PJ (2004) Effect of rifampicin on pravastatin pharmacokinetics in healthy subjects. *Br J Clin Pharmacol* **57**:181–187.

Lee JH, Chen HL, Chen HL, Ni YH, Hsu HY, and Chang MH (2006) Neonatal Dubin-Johnson syndrome: long-term follow-up and MRP2 mutations study. *Pediatr Res* **59**:584–589.

Maeda K (2015) Organic anion transporting polypeptide (OATP)1B1 and OATP1B3 as important regulators of the pharmacokinetics of substrate drugs. *Biol Pharm Bull* **38**:155–168.

Maeda K and Sugiyama Y (2008) Impact of genetic polymorphisms of transporters on the pharmacokinetic, pharmacodynamic and toxicological properties of anionic drugs. *Drug Metab Pharmacokinet* **23**:223–235.

Matsushima S, Maeda K, Kondo C, Hirano M, Sasaki M, Suzuki H, and Sugiyama Y (2005) Identification of the hepatic efflux transporters of organic anions using double-transfected Madin-Darby canine kidney II cells expressing human organic anion-transporting polypeptide 1B1 (OATP1B1)/multidrug resistance-associated protein 2, OATP1B1/multidrug resistance 1, and OATP1B1/breast cancer resistance protein. *J Pharmacol Exp Ther* **314**:1059–1067.

Nies AT and Keppler D (2007) The apical conjugate efflux pump ABCC2 (MRP2). *Pflugers Arch* **453**:643–659.

Niinuma K, Kato Y, Suzuki H, Tyson CA, Weizer V, Dabbs JE, Froehlich R, Green CE, and Sugiyama Y (1999) Primary active transport of organic anions on bile canalicular membrane in humans. *Am J Physiol* **276**:G1153–G1164.

Sharma P, Butters CJ, Smith V, Elsby R, and Surry D (2012) Prediction of the *in vivo* OATP1B1-mediated drug-drug interaction potential of an investigational drug against a range of statins. *Eur J Pharm Sci* **47**:244–255.

Shingaki T, Takashima T, Ijuin R, Zhang X, Onoue T, Katayama Y, Okauchi T, Hayashinaka E, Cui Y, Wada Y, et al. (2013) Evaluation of Oatp and Mrp2 activities in hepatobiliary excretion using newly developed positron emission tomography tracer [^{11}C]dehydropravastatin in rats. *J Pharmacol Exp Ther* **347**:193–202.

Shitara Y, Sato H, and Sugiyama Y (2005) Evaluation of drug-drug interaction in the hepatobiliary and renal transport of drugs. *Annu Rev Pharmacol Toxicol* **45**:689–723.

Singhvi SM, Pan HY, Morrison RA, and Willard DA (1990) Disposition of pravastatin sodium, a tissue-selective HMG-CoA reductase inhibitor, in healthy subjects. *Br J Clin Pharmacol* **29**: 239–243.

Takashima T, Hashizume Y, Katayama Y, Murai M, Wada Y, Maeda K, Sugiyama Y, and Watanabe Y (2011) The involvement of organic anion transporting polypeptide in the hepatic uptake of telmisartan in rats: PET studies with [^{11}C]telmisartan. *Mol Pharm* **8**: 1789–1798.

Takashima T, Kitamura S, Wada Y, Tanaka M, Shigihara Y, Ishii H, Ijuin R, Shiomi S, Nakae T, Watanabe Y, et al. (2012) PET imaging-based evaluation of hepatobiliary transport in humans with (15*R*)-^{11}C-TIC-Me. *J Nucl Med* **53**:741–748.

Takashima T, Nagata H, Nakae T, Cui Y, Wada Y, Kitamura S, Doi H, Suzuki M, Maeda K, Kusuhara H, et al. (2010) Positron emission tomography studies using (15*R*)-16-*m*-[^{11}C]tolyl-17,18,19,20-tetranorisocarbacyclin methyl ester for the evaluation of hepatobiliary transport. *J Pharmacol Exp Ther* **335**:314–323.

Takashima T, Wu C, Takashima-Hirano M, Katayama Y, Wada Y, Suzuki M, Kusuhara H, Sugiyama Y, and Watanabe Y (2013) Evaluation of breast cancer resistance protein function in hepatobiliary and renal excretion using PET with ^{11}C-SC-62807. *J Nucl Med* **54**:267–276.

van Dijk R, Beuers U, and Bosma PJ (2015) Gene replacement therapy for genetic hepatocellular jaundice. *Clin Rev Allergy Immunol* **48**:243–253.

Watanabe T, Kusuhara H, and Sugiyama Y (2010) Application of physiologically based pharmacokinetic modeling and clearance concept to drugs showing transporter-mediated distribution and clearance in humans. *J Pharmacokinet Pharmacodyn* **37**:575–590.

Watanabe T, Kusuhara H, Watanabe T, Debori Y, Maeda K, Kondo T, Nakayama H, Horita S, Ogilvie BW, Parkinson A, et al. (2011) Prediction of the overall renal tubular secretion and hepatic clearance of anionic drugs and a renal drug-drug interaction involving organic anion transporter 3 in humans by *in vitro* uptake experiments. *Drug Metab Dispos* **39**:1031–1038.

Willmann JK, van Bruggen N, Dinkelborg LM, and Gambhir SS (2008) Molecular imaging in drug development. *Nat Rev Drug Discov* **7**:591–607.

Yoshida K, Maeda K, and Sugiyama Y (2013) Hepatic and intestinal drug transporters: prediction of pharmacokinetic effects caused by drug-drug interactions and genetic polymorphisms. *Annu Rev Pharmacol Toxicol* **53**:581–612.

Address correspondence to: Yasuyoshi Watanabe, RIKEN Center for Life Science Technologies, 6-7-3 Minatojima-minamimachi, Chuo-ku, Kobe, Hyogo 650-0047, Japan. E-mail: yywata@riken.jp